Contrib Mineral Petrol (1995) 122: 79–96

E. Zinngrebe · S. F. Foley

Metasomatism in mantle xenoliths from Gees, West Eifel, Germany: evidence for the genesis of calc-alkaline glasses and metasomatic Ca-enrichment

Received: 2 March 1995 / Accepted: 12 June 1995

Abstract We have investigated new samples from the Gees mantle xenolith suite (West Eifel), for which metasomatism by carbonatite melt has been suggested. The major metasomatic change is transformation of harzburgites into phlogopite-rich wehrlites. Silicate glasses are associated with all stages of transformation, and can be resolved into two major groups: a strongly undersaturated alkaline basanite similar to the host magma which infiltrated the xenoliths during ascent, and Si-Al-enriched, variably alkaline glass present exclusively within the xenoliths. Si-Al-rich glasses (up to 72 wt% SiO_2 when associated with orthopyroxene (Opx) are usually interpreted in mantle xenoliths as products of decompressional breakdown of hydrous phases like amphibole. In the Gees suite, however, amphibole is not present, nor can the glass be related to phlogopite breakdown. The Si-Al-rich glass is compositionally similar to glasses occurring in many other xenolith suites including those related to carbonatite metasomatism. Petrographically the silicate glass is intimately associated with the metasomatic reactions in Gees, mainly conversion of harzburgite orthopyroxene to olivine + clinopyroxene. Both phases crystallize as microlites from the glass. The chemical composition of the Si-Al-enriched glass shows that it cannot be derived from decompressional melting of the Gees xenoliths, but must have been present prior to their entrainment in the host magma. Simple mass-balance calculations, based on modal analyses, yield a possible composition of the melt prior to ascent of the xenoliths, during which glass + microlite patches were modified by dissolution of olivine, orthopyroxene and spinel. This parental melt is a calc-alkaline andesite (55–60 wt% SiO_2), characterized by high Al_2O_3 (ca. 18 wt%). The obtained composition is very similar to high-alumina, calc-alkaline melts that should form by AFC-type reactions between basalt and harzburgite wall rock according to the model of Kelemen (1990). Thus, we suggest that the Si-Al-enriched glasses of Gees, and possibly of other suites as well, are remnants of upper mantle hybrid melts, and that the Gees suite was metasomatized by silicate and not carbonatite melts. High-Mg, high-Ca composition of metasomatic olivine and clinopyroxene in mantle xenoliths have been explained by carbonatite metasomatism. As these features are also present in the Gees suite, we have calculated the equilibrium Ca contents of olivine and clinopyroxene using the QUI1F thermodynamical model, to show that they are a simple function of silica activity. High-Ca compositions are attained at low $a\ SiO_2$ and can thus be produced during metasomatism by any melt that is Opx-undersaturated, irrespective of whether it is a carbonatite or a silicate melt. Such low $a\ SiO_2$ is recorded by the microlites in the Gees Si-Al-rich glasses. Our results imply that xenolith suites cannot confidently be related to carbonatite metasomatism if the significance of silicate glasses, when present, is not investigated.

E. Zinngrebe[1] (✉) · S. F. Foley
Mineralogisch-Petrologisches Institut, Universität Göttingen, Goldschmidstrasse 1, D-37077 Göttingen, Germany

[1] *Present address:* FG Petrologie, Institut für angewandte Geophysik, Tu Berlin, EB 310, Strasse des 17. Juni 135, D-10623 Berlin, Germany

Editorial responsibility: J. Hoefs

Introduction

Metasomatism by percolating melts has long been recognized as a key process in the evolution of upper mantle rocks, yet the nature of the melts responsible for metasomatism is a matter of considerable uncertainty. In recent time, much emphasis has been put on carbonatitic melts, as they were found experimentally to coexist stably with peridotite parageneses at appropriate *P* and *T* (e.g. Wallace and Green 1988; Dalton and Wood 1993) and appear suitable as metasomatic agents due to their low viscosity and low dihedral angle with mantle phases (Watson et al. 1990). Mantle metasomatism by carbonatite melt has been postulated in a variety of geodynamic environments and inferred in a number of different spinel lherzo-

Table 1 Modal composition of xenoliths rich in clear glass and of clear glass patches (vol. %)

Sample Phase	Bulk xenoliths				Sample Phase	Clear glass patches					
	G112	G22	G77	G39		G112 Type IIa	G22 Type IIb	G77 Type IIa	G39 Type IIb	Type II	Type II
Olivine	70.4	59.1	59.1	73.3	Olivine	13	24	20	26	29	31
Orthopyroxene	17.4	19.7	29.9	Trace	Opx	0	1	0	3	0	0
Clinopyroxene	0.0	4.6	6.6	13.3	Cpx	24	31	31	33	41	25
Spinel	Trace	1.8	0.5	0.5	Spinel	5	1	3	2	Trace	Trace
Phlogopite	0.0	0.0	0.0	0.4	Glass	59	43	46	35	30	45
Clear glass + microlites	10.7	12.1	3.6	7.2							
Brown glass + microlites	1.6	2.6	0.3	5.2							
Sum	100	100	100	100							
Points	2000	2087	2216	2165							

lite xenolith suites (Yaxley et al. 1991; Dautria et al. 1992; Rudnick et al. 1993; Hauri et al. 1994; Thibault et al. 1992; Ionov et al. 1993). A problem with metasomatism by carbonatite melts is that the metasomatizing agent is inherently ephemeral due to the extreme mobility and reactivity of carbonate melts in peridotites (Watson et al. 1990). Only one study has reported direct observation of carbonate melt in mantle xenoliths (Ionov et al. 1993).

In contrast, silicate glasses are very frequently observed in xenoliths but have received decreasing attention as metasomatizing agents, being frequently discarded as post-entrainment alteration features (decompressional melting). One of the xenolith suites cited as being related to carbonatite metasomatism (e.g. Dalton and Wood 1993; Thibault et al. 1992) is that from Gees, West Eifel, Germany (Düren 1984; Lloyd et al. 1991), which at the same time is notable for the occurrence of silicate glass (Edgar et al. 1989) in the xenoliths. Here we present an investigation of new samples from this locality, in which we show that (1) there is no evidence for carbonatite metasomatism judging from petrography and phase compositions; (2) that a specific variety of the silicate glasses, which is similar to glasses often explained by decompressional melting, is derived from a melt present within the xenoliths prior to their ascent; (3) that this melt can be explained by silicate melt – wallrock reactions similar to those modelled by Kelemen (1990). Thus, the Gees suite may be interpreted as the result of silicate melt metasomatism only.

The Gees xenolith suite

The Gees xenoliths occur in scoria associated with a maar-type volcanic structure situated in the centre of the West Eifel volcanic province, a tight cluster of continental alkaline intraplate volcanics containing widely known xenolith localities (e.g. Dreiser Weiher and Meerfeld: Witt-Eickschen et al. 1993; Stosch and Seck 1980). The Gees suite is unique within the West Eifel province in that phlogopite is the only hydrous phase occurring, whereas amphibole is present in other Eifel suites. The xenolith-entraining magma is a highly undersaturated alkaline basanite belonging to the Foidite group of Mertes and Schmincke (1985). The xenoliths are centimetre to decimetre sized and frequently coated with a thin (<1 mm) glass layer, termed "jacket glass" by Edgar et al. (1989). They can be divided into two major groups: a harzburgite – lherzolite – wehrlite – dunite series representing upper mantle with a metamorphic and variable metasomatic history (group I xenoliths in the classification of Frey and Prinz 1978), and clinopyroxenites, phlogopite clinopyroxenites and orthopyroxenites (group II) that are interpreted as products of high-pressure crystallization within magmatic veins. We have collected about 150 fresh xenoliths in Gees and selected 26 representative nodules for detailed petrography. A general feature of the Gees suite is the high amount of composite xenoliths and the complexity of veining relationships within them. Of 22 group I xenoliths, only 8 are homogeneous, the remainder shows highly variable layering and magmatic veining. However, a detailed study of the vein-wallrock relationships is beyond the scope of this paper (see Lloyd et al. 1991). In the

Fig. 1a–f Metasomatic textures in the Gees xenoliths. Long side of figure is 6 mm in (**a**), (**b**), (**c**); 1.5 mm in (**d**)–(**f**) and 750 µm in (**g**) and (**h**). **a** Harzburgite G22, crossed polars. Fine-grained aggregates of olivine + clinopyroxene microlites in glass matrix at the rims of strained, undulose orthopyroxene porphyroclasts. Glass in these fine-grained aggregates is termed type IIb glass in this work. **b** Wehrlite G39, single polar. In the *right-hand* side, large clinopyroxene crystals with melt-inclusion-rich rims. *Left*, a fine-grained olivine + clinopyroxene microcumulate area, the matrix of which consists of clear glass. Glass also coates most grain boundaries of large clinopyroxenes. **c** Cpx dunite G109, single polar. Phlogopite + clinopyroxene stringers along the grain boundaries of olivine porphyroclasts. Note that inclusion-dusted olivine cores are discordantly cut by metasomatic veinlets. **d** Cpx dunite part, G5, single polar. Unstrained, inclusion-free olivine tablet grains replace a strained, inclusion-dusted olivine porphyroclast. Note that tablet grains grow from metasomatic phlogopite-clinopyroxene patch, and thin melt film on tablet grain surface (at *1*). **e** Harzburgite G22, single polar. Discordant type I glass veinlet (*1*), originating at the xenolith surface. Type IIa, clear glass coating olivine grain boundaries (*2*). Note rapid change of glass colour at contact between both types of glass (*3*), and clinopyroxene crystallizing from IIa glass coating (*4*). **f** Harzburgite G112, single polar. Type IIa glass + microlite patch exclusively bounded by olivine crystals. Most microlites are clinopyroxene. Note their skeletal habits and spinel microlites on resorbed olivine surfaces. Also, note continuous glass films on olivine surfaces extending from the patch (*1*). **g** Wehrlite G39, crossed polars. Orthopyroxene relict enclosed in olivine crystal. A silicate melt inclusion trail (*1*) crosses *left* to *right*. Note replacement rim of clinopyroxene developing on orthopyroxene where this is touched by the melt inclusion array *(2, bright)*. **h** Wehrlite G39, crossed polars. Orthopyroxene relict *(in extinction)*, enclosed in olivine, but completely encapsulated by a clinopyroxene rim. Compare Fig. **g**. Note radial cracks in olivine possibly due to decompression.

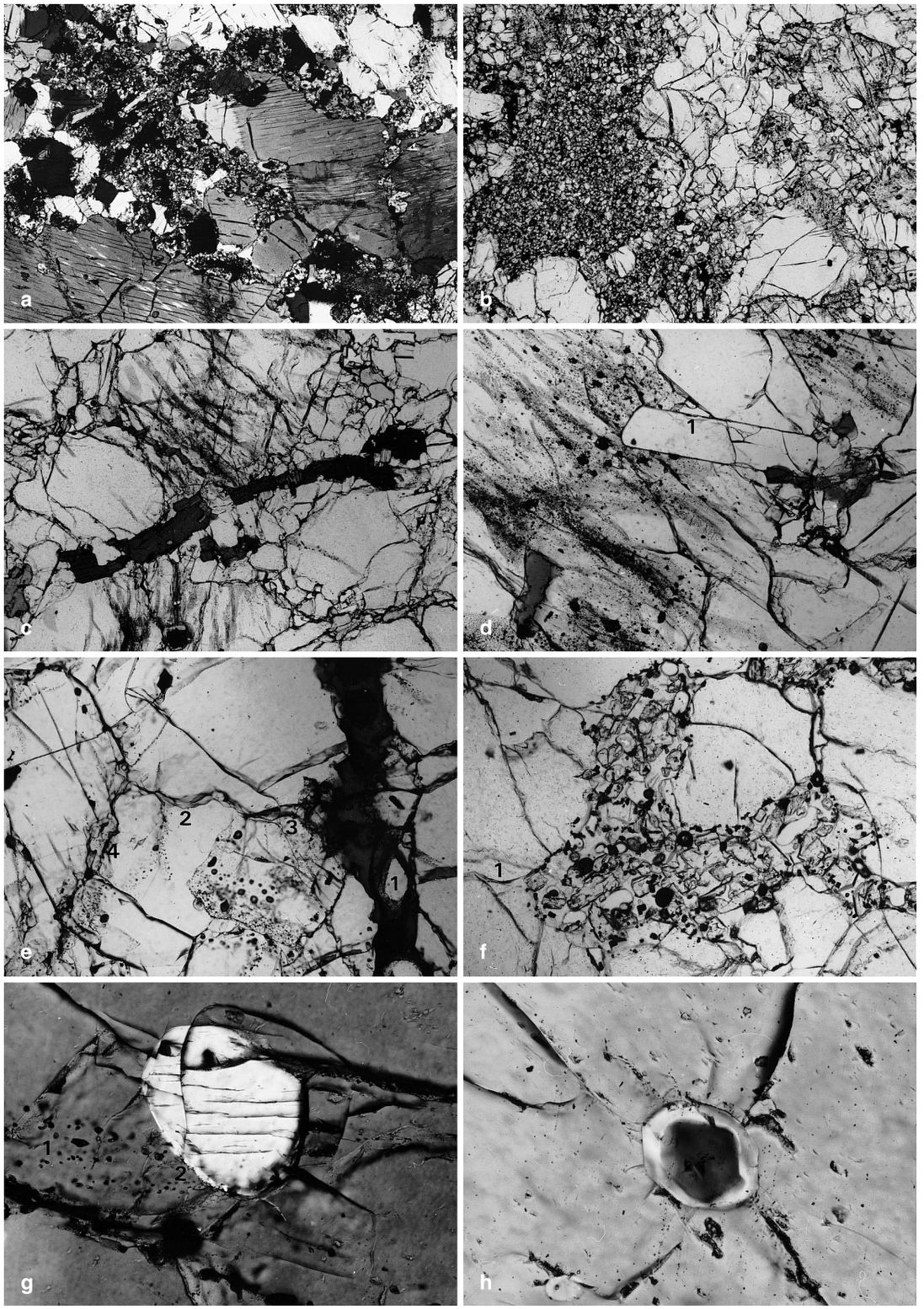
a
b
c
d
1
e
2
3
4
1
f
1
g
1
2
h

following petrography, we will use Opx and Cpx for orthopyroxene and clinopyroxene for brevity.

Petrography

Harzburgites

Six of the studied samples are harzburgites, three of which are homogeneous (G19, G22, G112). One sample contains a harzburgite-orthopyroxenite contact (G33), one is interlayered with olivine websterite and dunite (G24), and one shows a contact to olivine clinopyroxenite (G77). In general, the harzburgites are characterized by a coarse granular fabric of interlocking olivine + orthopyroxene, with grain sizes of 1–5 mm. All have primary, opaque (Cr-rich) or brown – translucent (Al-rich) spinel. In most harzburgites, large grains of Cpx (up to 1 mm in size) have been observed that appear to be in textural equilibrium with other phases and are judged to be "primary" (that is, older than metasomatic assemblages in the respective xenoliths; see Table 1 for modal analyses of three samples). The xenolith G112 does not contain any primary Cpx and is the most refractory of the investigated harzburgites. The textures of the harzburgites vary from equigranular to a sheared, strongly foliated texture (e.g. Fig. 1a). In sheared xenoliths, Opx forms elongated porphyroclasts with frequent kink bands and recrystallized rims. Olivine displays (100) deformation banding and signs of dynamic recrystallization. Hydrous phases (phlogopite) are very rare in harzburgite and always associated with infiltrated glasses (see below).

Clinopyroxene dunites and wehrlites

With 13 samples, Cpx-rich dunites and wehrlites make up the bulk of the Gees xenolith suite. Six of these (G5, G14, G18, G32, G48, G60) are veined by phlogopite-rich olivine clinopyroxenite, the others (G13, G20, G38, G39, G71, G108, G109) are more or less homogeneous. In general, recrystallized and highly deformed textures can be distinguished. Large, up to 2 mm sized olivine crystals dominate the texture, and in the deformed samples these show evidence of dynamic recrystallization. A distinct class of large, texturally old olivine grains is cut by numerous fluid and melt inclusion trails giving them a dusty appearance. These grains, which range in size from 100 μm to more than 1 mm, are replaced by tablet olivine grains which are nearly free of inclusions (Fig. 1d). In fully recrystallized samples, tablet grains make up the bulk of the xenolith volume.

In most samples Cpx + phlogopite occur as 0.1–1 mm thick stringers outlining the large olivines (Fig. 1c). There is a gradual transition between these intergranular stringers and discordant phlogopite clinopyroxenite veins. In most cases, small (50–100 μm) round or idiomorphic olivine grains occur within these stringers and are sometimes embedded in poikilitic Cpx. The phlogopites occur as large hypidiomorphic flakes, and sometimes cut discordantly through old olivine grains (Fig. 1c). Spinel is present in all Cpx dunite and wehrlite samples as rounded, opaque grains mantled by Cpx and less frequently by phlogopite, and as inclusions within olivine.

Several samples have conspicuous, millimetre sized symplectic intergrowths of Cpx + spinel surrounded by thick margins of phlogopite. These symplectites are often deformed, but in one sample, the outlines of a Cpx + spinel intergrowth perfectly mimick idiomorphic amphibole. This may indicate the former presence of amphibole which possibly has been consumed in a subsolidus reaction, thus providing a link between the Gees xenolith suite and other Eifel suites which have amphibole (Stosch and Seck 1980; Witt 1989).

Orthopyroxenites and olivine websterites

Three samples (G24, G33, G91) contain orthopyroxenite and one (G55) olivine websterite, always as a part of a composite xenolith. Veining relationships within individual xenoliths are very complex. One of them (G91, Table 1) contains an irregular area of orthopyroxenite with Cpx dunite, phlogopite wehrlite and quenched Ol-Cpx-glass cumulate as wallrock alternating within few centimeters. The orthopyroxenites are made up of mm sized, equant grains forming a cumulus texture, and are essentially monomineralic apart from opaque spinel and a few possibly primary olivines. As they show signs of Opx recrystallization and have irregular, recrystallized borders against their wall rocks, they are interpreted as high-pressure cumulates. No primary phlogopite or Cpx has been observed. The olivine websterite sample (G55) has a recrystallized equilibrium texture of interlocking, irregular olivine + Cpx + Opx grains of several 100 μm size.

Clinopyroxenites, olivine clinopyroxenites, phlogopite clinopyroxenites

Four xenoliths are composed entirely of clinopyroxenite, and five contain clinopyroxenite parts as veins within mantle wallrock. Two different types of clinopyroxenite exist: (1) dark-green clinopyroxene cumulates; (2) ophitic clinopyroxenites with light-green Cpx that resembles that within Cpx + phlogopite + granular olivine stringers in the Cpx-dunites and wehrlites. Within the first (dark-green) group, which is interpreted as magmatic cumulate, variation is present: Whereas some are essentially monomineralic with minor opaque spinel, one has a significant proportion of intergranular, apparently primary olivine and in another early cumulus Cpx is replaced by large poikilitic crystals of strongly coloured biotite. Magmatic zoning is preserved in this group. In contrast, the second (light-green) type of clinopyroxenite invariably is in contact with Cpx dunite or wehrlite within composite xenoliths. There are no sharp vein/wallrock contacts, but smooth transitions into clinopyroxene-phlogopite stringers within the host rock. The texture is comparatively fine grained (<1 mm), with Cpx and phlogopite either poikilitically enclosing granular olivine, or recrystallized to a granular fabric of all three minerals. The modal content of olivine varies but generally is low (see Table 1).

Glass-xenolith relationships

As noted in the Introduction and described by Edgar et al. (1989), many of the Gees xenoliths contain significant quantitites of glasses (see Table 1). These glasses and their significance are the main object of this study and are therefore described in detail. Two types of glass are discriminated according to colour and mode of occurrence as described in the following sections: type I, "brown glasses" (subdivided into Ia: jackets around xenoliths; Ib: discordant veins through xenoliths; Ic: glasses associated with phlogopite decomposition, mainly in cumulate clinopyroxenites) and type II, "clear glasses" (subdivided into IIa: inter-olivine glass patches in harzburgites; IIb: orthopyroxene-associated glass patches + inclusions in Opx; IIc: clear glass in dunites + wehrlites). At numerous terminations of clear glass-coated grain boundaries against discordant brown (type Ib) glass veins, the colour change occurs over distances of tens of microns, indicating only very limited interdiffusion between the two types of glass (Fig. 1e). In general, colour change can be used as a criterion to delimit areas of melt mixing in individual xenoliths.

a) Type I (brown) glasses

Thin layers of dark-brown glass enclose virtually all Gees xenoliths, being termed "jacket glass" following Edgar et al. (1989). It contains a high proportion of phenocrysts of green-coloured clinopyroxene and leucite of several 100 μm size. Additionally, there is a population of very small (<10 μm) skeletal microlites of clinopyroxene, leucite + spinel in the groundmass. With the exception of clinopyroxenites, all xenoliths are coated by a 100–200 μm thick continuous rim of clinopyroxene against this jacket glass. This rim discordantly replaces all xenolith phases and is strongly colour-zoned. The jacket glass itself is compositionally different from the scoria of the Gees maar (see Edgar et al. 1989).

The brown glass infiltrates the harzburgite, dunite and wehrlite xenoliths along discordant cracks (Fig. 1e) starting at xenolith surfaces. The glass within these cracks is petrographically identical to the jacket glasses, containing numerous large vesicles as well as some large, idiomorphic clinopyroxene crystals. The surfaces of brown glass against olivine are highly ragged and consist of numerous idiomorphic pits and grooves of 1–5 μm size, which often are lined with tiny spinel crystals. Where brown glass is in contact with Cpx originally crystallized from type II glass as microlites (see below), the Cpx is invariably strongly zoned (becoming Ti-, Al-enriched) and sometimes resorbed. The infiltrating brown glass veins contain a specific association of very small (<5 μm) quench crystals (Cpx, leucite, spinel) that can be distinguished by size and habit from the larger microlites (phenocrysts). A characteristic of the brown glass is the frequent occurrence of sulfide globules.

Within harzburgites and orthopyroxenites, type I, brown glass occurs frequently in the form of pseudosecondary melt inclusion trails or single melt inclusions of up to 20 μm size in all minerals. Minute ilmenite and sulfide have been identified in these inclusions. The "dusty" appearance of old olivine grains in Cpx-dunites (see above) also is caused by many small inclusions which however, due to their small size (<5 μm) and apparent reactions with the host, cannot unequivocally be identified as melt or fluid inclusions in most cases. Significantly, brown melt inclusions within accessory clinopyroxene in one harzburgite and within olivine in one wehrlite (G39) contained phlogopite crystals. In one inclusion in wehrlite G39, a tiny hexagonal daughter crystal, possibly apatite, occurs.

Within the clinopyroxenite xenoliths (or xenolith parts), intergranular brown glass sometimes is present on grain boundaries and as somewhat larger melt pools around phlogopites. If glass is present in the clinopyroxenites, paragenetically identical stringers in dunite wall rock in the same xenolith can be glass-free (e.g. G5). Phlogopite flakes in some Cpx-dunites and wehrlites are lined by thin glass rims and display rounded dissolution morphologies. The surrounding glass (type Ic) is brown and contains frequent small spinel quench crystals. However, there are samples (e.g. wehrlite G39) where phlogopite shows no signs of incipient melting.

b) Type II (clear) glasses

The second main type of glass in the Gees xenolith suite occurs exclusively in the interior of xenoliths. It is conspicuously associated with metasomatic reactions, and it does not occur in clinopyroxenites (high-pressure magmatic cumulates). This colourless glass is most abundant in the harzburgites, a significant volume of which can consist of glass + olivine + Cpx patches, although essentially identical patches also occur in Cpx dunites and wehrlites (see Table 1). In the harzburgites, the glass patches occur interstitially at the junctions of olivine grains (type IIa, Fig. 1f) or are situated at the margins of Opx porphyroclasts (type IIb; see Fig. 1a). The patches vary in size from several hundred μm to several mm and are filled with aggregates of perfectly idiomorphic olivine + Cpx forming blocky intergrowths or a microcumulate texture, with individual crystals varying in size from tens to hundreds of μm. Within the glass patches, large vesicles occur indicating that a significant amount of volatiles was dissolved in the melt prior to decompression. Typically the glass patches are connected by thin (10 μm or less) channels of interstitial clear glass coating the grain boundaries of olivine. The surfaces of these grain boundary channels are gently curved and smooth, indicating no obvious reaction relationship. The Opx invariably has ragged margins against glass patches and its surface is lined with newly formed olivine + clinopyroxene crystals. Typically, this Opx decomposition extends into the interior of Opx porphyroclasts along kink boundaries or along lamellar planes. Exclusively in these Opx-associated glass patches, orthopyroxene has been observed as a rare microlite phase. Pseudosecondary trails of glass inclusions that cut through Opx contain large olivine + clinopyroxene crystals, and skeletal olivine lamellae with thin coatings of clear glass are also present within Opx. Primary lobate spinel grains in the harzburgites are invariably embedded in glass pools and have thick margins consisting of spinel + glass symplectites.

In the dunites and wehrlites, clear glass lines many olivine-olivine grain boundaries (type IIc) and in deformed dunites with strong deformation textures, disaggregation of strained olivine into small (<100 μm) neoblasts with interstitial glass has been observed. Glass inclusions and coatings of ≈10 μm thickness also decorate high-angle subgrain boundaries separating (100) lamella fans within olivine cores. Small Cpx crystals may be associated with these glasses within olivine porphyroclasts, implying that the wetting of subgrain boundaries by glass was not merely caused by grain-boundary dilatation during pressure decrease, but involved some metasomatic reaction. An origin of the Cpx dunites and wehrlites by metasomatic transformation from Opx-bearing samples (lherzolites or harzburgites)

is further indicated by small relic Opx inclusions in olivine porphyroclasts in many samples, which frequently are rimmed by thin margins of Cpx (Fig. 1g, h). In wehrlite G39, direct evidence for the conversion of an Opx relic in olivine into Cpx by reaction with melt has been observed (see Fig. 1g). Further, large Cpx crystals in the wehrlites have rims dusted with clear glass inclusions, and olivine-Cpx microcumulate areas with interstitial clear glass similar to the type IIa harzburgite glass patches occur (see Fig. 1b).

Implications from petrography for the genesis of the glasses

Important conclusions about the reaction relationships visible in the Gees xenoliths can be deduced from the above petrographic observations. The enclosure of the xenoliths in type I (brown) glasses, in contrast to the purely intraxenolithic occurrence of type II (clear) glass, demonstrates that the clear glass must either have been present before entrainment of the xenoliths in the host magma, or be the product of decompressional melting of the xenolith's interior, or a combination of both. Düren (1984) has argued that the clear glasses were the result of amphibole melting, based on textural similarity to glass in other Eifel suites where amphibole melting has been demonstrated. However, amphibole is completely absent from the Gees xenoliths, and nearly glass-free and Cpx-poor harzburgites show no trace of amphibole, arguing against a role of decompressional amphibole breakdown in the genesis of clear glasses. The same is indicated by our observation of conversion of Opx to Cpx by reaction with type II melt and precipitation of Cpx within olivine porphyroclasts during type II melt infiltration along subgrain boundaries. Thus the abundance of Cpx phenocrysts in type II glass patches in harzburgites as well as the coexistence of Cpx + olivine in a *single* type II melt inclusion in Opx demonstrates that there is a true metasomatic component to these patches which cannot be derived internally from the xenoliths. Therefore, the melt variety represented by the type II glasses must have been present within the xenoliths at mantle depth, although the melt composition may have been changed during subsequent eruption.

In agreement with the results of Lloyd et al. (1991), our petrographic observations suggest that the essential metasomatic change displayed by the Gees suite is the transformation from harzburgite to wehrlite/dunite. An intimate association between *silicate* glasses (type II) and modal metasomatism is apparent which was not explained by Thibault et al. (1992) in their proposal of a carbonatite-related genesis for the Gees suite. To investigate further the connection between silicate glasses and metasomatism and to elucidate possible roles of post-entrainment decompressional overprint, we selected seven xenoliths, representing different stages of the conversion and displaying all essential glass textures, for detailed microprobe analysis. These xenoliths are three harzburgites (G112, G22, G77 in order of increasing metasomatic overprint), a wehrlite (G39), 3 composite xenoliths (G5: Cpx dunite with phlogopite clinopyroxenite vein; G91: orthopyroxenite with wehrlite wall rock; G97: clinopyroxenite with wehrlite-lherzolite wall rock; see Table 1). Modal analyses of the four homogeneous xenoliths, which are the most glass-rich, are given in Table 1 together with estimates of the modal composition of the clear glass patches.

Analytical methods

Electron microprobe analyses of minerals and glasses concentrated on the relations between the various glasses and primary and introduced phases. Wavelength-dispersive analyses were performed with an automated Jeol 8600 microprobe at the Institut voor Aardwetenschappen, University of Utrecht. Operating conditions were an accelerating voltage of 25 kV, a beam current of 30 nA and peak counting times of 30 seconds per element for most analyses. An additional session on sample G97 used 10 nA/60 seconds. Natural and synthetic minerals were used as standards. Repeated analyses of diopside and forsterite revealed no systematic errors with the exception of somewhat high analytical totals for forsterite. Precision of analyses is $\pm 0.5\%$ (relative) for major elements and better than $\pm 10\%$ (relative) for most minor elements. The CaO in olivine has been analysed with ± 0.01 wt% absolute error ($1\,\sigma$) at the 0.1 wt% level. Glass analyses were obtained at the above conditions with a defocused beam of 5 µm where possible. Due to the small size of interstitial glasses many analyses could only be performed with fully focussed beam (2 µm). Analytical totals of focussed analyses are not systematically lowered, and online observation of sodium count rates revealed only minor alkali loss.

Results

Mineral compositions

Our microprobe analyses concentrate on the relationship between the xenolith phases and the intraxenolith glasses; they are given xenolith by xenolith in Tables 2 to 7. For general data on the primary phase compositions of the Gees suite the reader is referred to Lloyd et al. (1991) whose results are summarized here. Within the harzburgites, a positive correlation exists between modal olivine content and Mg-# [=Mg/(Mg+Fe)] of olivine, which range from 0.88 to 0.92. The Mg-# of phases in the Cpx-enriched lherzolites and of the dunite-wehrlite group tend to be lower, with minimum values of 0.82. Silicates in Cpx-bearing dunites can have Mg-# as high as 0.90. In general, Opx, olivine and Cpx have equilibrated according to their Mg-# (Ol $\approx$ Opx$<$Cpx). Edgar et al. (1989) and Lloyd et al. (1991) found that stringer-forming, metasomatic Cpx and phlogopite in the lherzolites and wehrlites are also in Fe-Mg exchange equilibrium with their hosts, and lower in Mg-# in the wehrlites due to the generally lower Mg-# of phases in these xenoliths. They distinguished different generations of Cpx according to their Ti and Al contents: The cumulate clinopyroxenites show a strong, the wehrlite clinopyrox-

Table 2 Composition of phases in harzburgite G112 (FeO_T total iron as FeO)

Phase petrography	Olivine microlites IIb glass	Olivine rims+ microlites IIa glass	Olivine primary (cores)	Opx primary (cores)	Opx rims+ microlites IIb glass	Cpx core of microlite IIa glass	Cpx rim of microlite IIa glass	Cpx microlites IIb glass	Spinel microlite IIa glass	Glass IIa between olivines	Glass IIb around Opx	Glass inclusion trail in Opx	Glass olivine lamella in Opx	Glass jacket around xenolith
No. of analyses	2	3	2	3	4	1	1	3	1	3	3	1	1	2
SiO_2	41.60	41.78	41.25	57.36	57.75	52.05	51.79	54.00	0.02	60.59	71.47	66.77	71.99	42.77
TiO_2	0.00	0.00	0.00	0.02	0.01	0.07	0.08	0.04	0.07	0.18	0.10	0.05	0.07	3.15
Al_2O_3	0.02	0.03	0.00	1.78	1.56	4.52	4.35	2.31	28.32	21.90	16.77	17.4	13.81	16.77
Cr_2O_3	0.07	0.09	0.01	0.30	0.26	1.26	1.10	1.31	38.02	0.02	0.01	0.03	0.01	0.00
FeO_T	8.44	8.57	8.69	6.04	5.89	2.86	3.09	3.03	16.44	3.29	1.81	2.84	2.34	10.95
MnO	0.12	0.13	0.14	0.14	0.14	0.06	0.08	0.07	0.21	0.04	0.02	0.06	0.04	0.21
NiO	0.25	0.38	0.41	0.07	0.07	0.00	0.00	0.05	0.18	0.01	0.00	0.00	0.01	0.01
MgO	50.68	50.75	50.33	34.86	35.07	16.76	16.35	18.91	16.61	2.85	1.66	2.26	2.02	5.26
CaO	0.15	0.22	0.07	0.37	0.48	22.36	22.81	20.31	0.17	5.20	1.96	1.51	0.98	13.32
Na_2O	0.00	0.01	0.00	0.00	0.00	0.65	0.66	0.73	0.04	1.21	0.62	1.35	1.46	2.92
K_2O	0.00	0.00	0.00	0.00	0.00	0.01	0.02	0.00	0.01	1.27	1.09	1.82	2.13	3.29
Cl	0.00	0.00	0.00	0.00	0.00	0.00	0.01	0.00	0.00	0.33	0.22	0.28	0.18	0.27
Σ	101.33	101.96	100.89	100.93	101.22	100.6	100.34	100.75	100.09	96.89	95.73	94.37	95.04	98.88
Mg-#	0.915	0.913	0.912	0.911	0.914	0.913	0.904	0.918	0.736[a]	0.616	0.632	0.600	0.624	0.483
(Na+K)/Al										0.154	0.131	0.241	0.341	0.498

[a] Based on Fe^{2+} from stoichiometry in spinel

Table 3 Composition of phases in harzburgite G22 (FeO_T total iron as FeO)

Phase petrography	Olivine primary	Olivine micro-lites IIb glass	Opx primary	Opx micro-lite IIb glass	Spinel primary (cores)	Spinel glass sym-plektite	Cpx primary core	– zoned vs melt (start)	– zoned vs melt (rim)	Cpx micro-lites IIa glass	Cpx micro-lites IIb glass	Cpx micro-lite I glass	Glass type I discor-dant	Glass at zoned Cpx	Glass spinel sym-plektite	Glass IIa	Glass IIb
No. of analyses	18	3	1	1	2	2	10	1	2	1	2	1	5	5	1	4	3
SiO_2	41.21	41.32	56.16	57.72	0.00	0.00	53.33	51.17	49.18	51.49	53.88	53.76	45.09	50.09	51.90	53.74	72.02
TiO_2	0.00	0.00	0.02	0.02	0.02	0.15	0.11	0.67	1.45	0.23	0.13	0.20	2.70	1.68	0.35	1.03	0.15
Al_2O_3	0.00	0.01	3.53	0.43	48.75	38.85	2.62	4.44	5.58	5.63	2.94	3.27	17.58	19.97	21.41	21.55	15.42
Cr_2O_3	0.00	0.06	0.39	0.34	17.91	28.15	0.57	1.08	0.90	1.37	1.29	0.72	0.01	0.00	0.45	0.00	0.01
FeO_T	9.46	9.02	6.41	5.70	14.03	13.84	2.33	3.28	3.91	2.86	3.16	3.13	9.82	6.85	3.90	4.37	1.78
MnO	0.13	0.16	0.14	0.14	0.13	0.18	0.07	0.06	0.09	0.04	0.13	0.09	0.15	0.12	0.05	0.05	0.04
NiO	0.35	0.19	0.09	0.09	0.33	0.21	0.04	0.05	0.05	0.05	0.04	0.08	0.03	0.02	0.00	0.02	0.01
MgO	49.65	50.04	34.17	33.44	19.45	19.01	16.90	16.30	14.78	15.95	18.78	17.61	4.66	3.96	3.43	2.96	1.50
CaO	0.05	0.15	0.29	1.74	0.02	0.03	23.92	21.77	23.58	22.92	19.72	21.83	11.47	9.01	7.92	6.77	1.09
Na_2O	0.01	0.01	0.00	0.11	0.01	0.01	0.35	0.65	0.42	0.82	0.84	0.61	3.04	2.98	3.80	3.04	1.27
K_2O	0.00	0.00	0.00	0.00	0.00	0.01	0.00	0.01	0.00	0.00	0.01	0.00	3.01	2.94	3.81	3.75	1.90
Cl	0.00	0.00	0.00	0.00	0.00	0.00	0.00	0.00	0.01	0.00	0.01	0.00	0.31	0.34	0.44	0.38	0.16
Σ	100.88	100.95	101.20	99.73	100.62	100.41	100.23	99.48	99.92	101.36	100.90	101.30	97.86	97.96	97.46	97.65	95.35
Mg-#	0.903	0.908	0.905	0.913	0.780[a]	0.790[a]	0.928	0.918	0.871	0.909	0.914	0.909	0.478	0.524	0.628	0.564	0.616
(Na+K)/Al													0.469	0.405	0.485	0.420	0.269

[a] Based on Fe^{2+} from stoichiometry in spinel

Table 4 Composition of phases in harzburgite G77 (FeO_T total iron as FeO0

Phase petrography	Olivine primary	Olivine rim+ microlite II glass	Olivine micro-cumulus area	Opx primary	Opx rim vs IIb glass	Opx in melt inclusion in olivine	Cpx micro-cumulus area	Cpx reactional aggregate	Cpx microlite in II glass	Cpx microlite I glass (jacket)	Glass II, inclusion in Cpx	Glass II, inclusion in Opx	Glass II, inclusion in Ol	Glass type IIb patch	Glass type IIa patch	Glass discordant vein	Glass type I, jacket
No. of analyses	2	2	2	2	1	1	2	4	1	1	1	2	2	4	2	2	1
SiO_2	40.99	40.79	40.91	58.45	58.40	58.02	54.52	54.44	55.56	43.45	63.92	60.65	60.59	70.77	59.23	63.14	41.91
TiO_2	0.00	0.00	0.01	0.03	0.08	0.07	0.13	0.11	0.25	3.75	0.65	0.28	0.94	0.80	0.68	1.19	3.15
Al_2O_3	0.02	0.00	0.01	0.60	0.49	0.45	1.47	1.35	0.42	8.41	18.01	16.37	16.24	12.26	17.26	11.95	16.29
Cr_2O_3	0.03	0.05	0.01	0.24	0.31	0.16	0.82	1.48	0.98	0.00	0.04	0.03	0.02	0.02	0.04	0.03	0.00
FeO_T	11.92	11.46	12.76	6.98	6.97	6.91	3.86	3.72	3.86	8.12	4.25	4.92	4.69	3.82	5.25	4.05	10.54
MnO	0.27	0.24	0.35	0.20	0.19	0.18	0.17	0.19	0.15	0.10	0.00	0.10	0.11	0.08	0.13	0.06	0.22
NiO	0.25	0.18	0.23	0.08	0.09	0.03	0.04	0.03	0.05	0.01	0.00	0.03	0.02	0.01	0.02	0.02	0.00
MgO	48.01	48.10	47.41	34.71	33.89	34.82	17.42	17.55	18.97	11.41	0.99	3.53	2.44	2.75	2.27	2.75	4.97
CaO	0.14	0.20	0.21	0.60	1.30	0.95	21.42	20.95	20.27	23.79	1.20	2.00	3.56	1.32	2.28	1.70	12.45
Na_2O	0.01	0.01	0.01	0.08	0.11	0.08	0.83	1.05	0.74	0.38	1.50	1.35	1.48	1.24	1.79	4.50	3.28
K_2O	0.00	0.01	0.00	0.01	0.00	0.01	0.00	0.00	0.00	0.06	2.29	2.34	2.15	1.50	2.89	8.07	3.29
Cl	0.01	0.01	0.01	0.00	0.01	0.00	0.00	0.01	0.00	0.00	0.13	0.22	0.37	0.09	0.13	0.12	0.31
Σ	101.64	101.02	101.90	101.96	101.84	101.68	100.67	100.87	101.25	99.48	92.98	91.78	92.59	94.64	91.94	97.55	96.41
Mg-#	0.878	0.882	0.869	0.899	0.897	0.900	0.889	0.894	0.898	0.715	0.293	0.561	0.481	0.562	0.435	0.548	0.457
(Na+K)/Al											0.275	0.290	0.293	0.298	0.352	1.350	0.550

Table 5 Composition of phases in wehrlite G39 (FeO_T total iron as FeO)

Phase petrography	Olivine primary	Olivine micolites +rims, II glass	Opx relic in olivine	Cpx cores	Cpx micolites +rims, II glass	Cpx zoned to glass I (start)	Cpx zoned to glass I (rims)	Cpx microlite jacket (I) glass	Phlogopite idiomorphic flakes	Spinel microlite type I glass	Glass II, with olivine +Cpx	Glass II, included in Cpx	Glass I, discordant	Glass I, dissolving olivine	Glass I, at xenolith rim	Glass jacket (type I)
No. of analyses	5	7	1	11	4	1	3	1	2	1	4	2	4	1	1	2
SiO_2	40.86	40.60	57.08	52.94	53.59	46.98	49.35	43.07	38.32	0.00	59.74	60.48	40.68	39.11	41.76	41.34
TiO_2	0.01	0.02	0.17	0.45	0.46	1.63	1.43	4.00	4.07	2.69	1.84	1.56	3.20	2.74	3.27	3.25
Al_2O_3	0.02	0.03	0.51	2.35	1.07	7.16	4.66	8.67	15.78	21.05	18.27	17.88	15.92	13.72	16.12	16.07
Cr_2O_3	0.02	0.03	0.18	0.82	0.79	0.77	0.92	0.01	2.21	34.03	0.00	0.02	0.00	0.01	0.00	0.00
FeO_T	11.06	11.08	7.37	3.38	3.61	5.25	4.38	7.44	5.53	27.72	3.95	3.85	10.81	10.06	11.41	11.20
MnO	0.20	0.19	0.22	0.09	0.11	0.05	0.07	0.08	0.03	0.31	0.04	0.03	0.19	0.17	0.26	0.22
NiO	0.32	0.33	0.09	0.07	0.05	0.00	0.03	0.00	0.24	0.27	0.01	0.01	0.01	0.04	0.04	0.00
MgO	48.21	48.16	33.25	17.15	17.59	13.86	15.12	11.69	20.56	14.09	2.52	2.22	5.05	10.51	4.68	5.32
CaO	0.17	0.26	1.57	21.99	21.56	23.63	23.72	24.26	0.06	0.08	3.59	2.30	13.17	10.55	14.58	13.55
Na_2O	0.00	0.01	0.08	0.81	0.66	0.39	0.50	0.28	0.35	0.00	2.05	1.91	3.26	4.14	2.52	2.94
K_2O	0.00	0.00	0.00	0.01	0.02	0.01	0.01	0.00	7.32	0.04	2.62	2.52	3.38	5.04	2.57	3.36
Cl	0.00	0.00	0.00	0.00	0.00	0.00	0.00	0.00	0.02	0.01	0.14	0.13	0.30	0.25	0.28	0.25
Σ	100.87	100.70	100.52	100.05	99.50	99.73	100.18	99.50	94.48	100.29	94.75	92.88	95.96	96.34	97.49	97.48
Mg-#	0.886	0.886	0.889	0.900	0.897	0.825	0.860	0.737	0.869	0.475[a]	0.532	0.507	0.454	0.639	0.422	0.459
(Na+K)/Al											0.340	0.328	0.567	0.894	0.430	0.527

[a] Based on Fe^{2+} from stoichiometry in spinel

Table 6 Composition of phases in xenoliths G5 and G91 (FeO_T total iron as FeO)

	G5 Wehrlite part							G91 Orthopyroxenite part					
Phase petrography	Olivine dusted old grains	Olivine clear neoblast	Biotite metasomatic stringer	Cpx metasomatic	Cpx xenolith selvage	Cpx microlite jacket glass	Glass jacket (type I)	Opx cores	Opx rim to type II glass	Olivine microlite type II glass	Cpx microlite type II glass	Glass II, inclusion in Opx	Glass II, grain boundaries
No. of analyses	14	2	2	3	1	1	2	2	1	2	2	1	1
SiO_2	40.47	40.75	38.47	52.20	48.01	47.15	40.56	58.33	58.04	41.13	54.34	59.73	66.71
TiO_2	0.01	0.02	2.60	0.46	2.05	2.69	2.51	0.06	0.07	0.01	0.34	0.53	0.86
Al_2O_3	0.03	0.02	16.35	3.24	5.82	5.76	16.41	0.68	0.60	0.01	1.45	15.47	13.03
Cr_2O_3	0.01	0.01	1.51	0.79	0.70	0.01	0.01	0.27	0.34	0.04	1.76	0.01	0.01
FeO_T	13.10	12.87	6.62	3.87	5.22	6.68	10.36	6.95	7.18	11.68	3.78	3.33	3.18
MnO	0.49	0.47	0.10	0.18	0.09	0.08	0.23	0.20	0.25	0.26	0.17	0.09	0.07
NiO	0.39	0.38	0.19	0.03	0.00	0.00	0.02	0.06	0.10	0.22	0.03	0.01	0.01
MgO	46.37	46.48	21.59	15.71	14.01	13.60	3.46	34.46	33.94	48.29	17.56	3.32	2.17
CaO	0.28	0.28	0.04	23.49	24.00	24.35	10.82	0.62	0.87	0.12	20.42	1.50	1.45
Na_2O	0.01	0.00	0.25	0.54	0.36	0.26	5.84	0.10	0.11	0.00	1.32	6.19	4.00
K_2O	0.00	0.00	7.26	0.00	0.00	0.00	6.85	0.00	0.00	0.00	0.00	7.01	5.36
Cl	0.00	0.00	0.02	0.00	0.01	0.00	0.40	0.00	0.00	0.00	0.00	0.16	0.11
Σ	101.14	101.26	94.97	100.52	101.27	100.58	97.43	101.71	101.50	101.75	101.14	97.35	96.94
Mg-#	0.863	0.866	0.853	0.879	0.827	0.784	0.373	0.898	0.894	0.881	0.892	0.640	0.549
(Na+K)/Al							1.037					1.149	0.950

enes a lesser enhancement in Ti+Al. Significantly both have similar Ti/Al ratios of 1:5. Absolute concentrations of TiO_2 reach >2 wt% and >1 wt%, respectively. The maximum Al_2O_3 is attained in the cumulate clinopyroxenes (clinopyroxenites) with >8 wt%. In contrast, the harzburgite-lherzolite clinopyroxenes are low in TiO_2 (<0.2 wt%) and Al_2O_3 (commonly <1.5 wt%).

Olivine

The three harzburgites we studied (G112, G22, G77) have primary olivines with Mg-# of 0.92 to 0.87 and thus span the range of Mg# found by the previous investigators. Sample G112, which is petrographically least affected by metasomatism and Cpx-free apart from microlites in type II glass patches, has the most refractory olivine composition (Table 2). Harzburgite G77 is very rich in secondary (metasomatic) Cpx, and has the most Fe-rich olivine (Table 4). The CaO-Mg-# relations for olivine in all samples are given in Fig. 2, which also shows the comparatively Fe-rich composition of the lherzolite wallrock to clinopyroxenite in composite xenolith G97 (Mg-# of olivine 0.83–0.85, Table 7). The Mg-# of silicates in the wehrlite G39 and Cpx dunite G5 are intermediate between those of this lherzolite and of the harzburgites (see Tables 5, 6).

The Ca content of olivine rims against intergranular type IIa and against discordant type I glass is slightly, but systematically enchanced by up to 0.2–0.3 wt%. These Ca-enriched rims are restricted to 20–30 μm thickness. They are interpreted to represent diffusive re-equilibration of olivine against the Ca-bearing glasses, which is supported by their similarity to the compositions of olivine microlites within the clear intergranular glass. The Ni and Mn contents and, significantly, the Mg-# in both does not deviate strongly from the primary olivine composition. In the harzburgites, phenocrysts of olivine in type IIb (Opx-associated) and IIa (inter-olivine) glass patches differ significantly in Ni contents (harzburgite samples): olivine microlites are significantly depleted in Ni when situated in IIb patches. The Mg-# of IIa glass olivine microlites is usually among the highest found in individual samples (see Tables 2–4).

Orthopyroxene

Orthopyroxene compositions are shown in Fig. 3 and given in Tables 2–7. The Mg-# of Opx porphyroclasts is similar to that of olivine in the relatively refractory harzburgites G22 and G112, it is however significantly higher in G77 (0.90 compared to olivine: 0.87–0.88). Similarly, in the lherzolite wall rock of the clinopyroxenite G97, large Opx porphyroclasts have Mg-# 0.87 decreasing in smaller neoblasts to 0.85, whereas olivine is as Fe-rich as $Fo_{0.83}$. Here, the Opx neoblasts are three times as Ca-rich as the porphyroclasts.

In all Opx-bearing samples, Opx rims in contact with clear glass (type IIb) are also Ca-enhanced with little change or even an increase in Mg-#. Rare microphenocrysts of Opx in type IIb glass patches have the highest CaO contents ($\approx$1.8 wt%) comparable to that of a single Opx relict in an olivine in the wehrlite G39. Further, there are notable zonations in the minor element contents of Opx in contact with type II glass, the most significant of which is a decrease of Al and Cr. Orthopyroxenes in the two most refractory harzburgites, G22 and G112, have the highest Al_2O_3 and Cr_2O_3 concentrations of the primary Opx (see Tables 2, 3), comparable to that of

Table 7 Composition of phases in composite xenolith G97. Xenolith G97 consists of the following zones: phlogopite clinopyroxenite, separated by a thin layer of massive phlogopite and a few mm of wehrlite from porphyroclastic lherzolite wall rock (FeO_T total iron as FeO)

Phase petrography	Olivine primary lherzolite part	Olivine wehrlite part	Olivine microlite biotite zone	Olivine microlite clinopyroxenite part	Opx porphyroclast lherzolite part	Opx small in lherzolite part	Cpx lherzolite part	Cpx wehrlite part	Cpx biotite zone	Cpx clinopyroxenite cores	Cpx clinopyroxenite rims	Spinel lherzolite part	Glass biotite zone	Glass clinopyroxenite	Glass[b] lherzolite part type IIb
No. of analyses	8	7	2	1	4	9	12	11	6	2	1	7	4	2	2
SiO_2	40.35	40.19	40.21	40.20	57.14	57.43	54.60	54.27	52.00	53.27	49.57	0.00	44.36	41.35	64.84
TiO_2	0.00	0.01	0.10	0.07	0.03	0.05	0.10	0.17	0.81	0.41	1.27	1.24	3.81	3.89	1.20
Al_2O_3	0.00	0.01	0.06	0.04	0.54	0.38	0.93	1.05	3.37	1.65	5.20	5.06	18.46	18.09	12.12
Cr_2O_3	0.01	0.01	0.04	0.04	0.09	0.10	0.69	0.58	0.26	0.46	0.42	42.36	0.02	0.03	0.00
FeO_T	15.26	15.95	15.05	14.16	8.77	9.52	4.83	4.56	5.81	5.31	6.32	38.13	7.26	7.94	4.43
MnO	0.39	0.45	0.30	0.25	0.26	0.39	0.22	0.21	0.15	0.14	0.13	0.56	0.14	0.12	0.10
NiO	0.17	0.10	0.05	0.06	0.04	0.04	0.02	0.02	0.01	0.01	0.00	0.07	0.00	0.01	0.00
MgO	45.30	44.53	44.40	45.47	33.41	32.25	17.14	16.67	14.55	15.33	13.71	7.86	4.43	4.48	2.46
CaO	0.12	0.20	0.54	0.64	0.38	1.08	20.56	22.03	21.92	23.21	22.28	0.00	9.36	9.06	1.91
Na_2O	0.01	0.02	0.02	0.01	0.08	0.08	1.06	0.80	0.95	0.86	1.09	0.02	2.87	3.49	1.42
K_2O	0.00	0.00	0.02	0.01	0.00	0.00	0.00	0.00	0.00	0.01	0.01	0.00	5.22	8.13	7.16
Cl	0.00	0.00	0.01	0.00	0.00	0.00	0.00	0.00	0.00	0.01	0.00	0.00	0.16	0.18	0.00
Σ	101.60	101.46	100.76	100.95	100.72	101.32	100.13	100.35	99.82	100.63	100.00	95.29	96.09	96.75	95.66
Mg-#	0.841	0.833	0.840	0.851	0.872	0.858	0.864	0.867	0.817	0.837	0.795	0.411[a]	0.521	0.501	0.498
(Na+K)/Al													0.562	0.804	0.832

[a] Based on Fe^{2+} from stoichiometry in spinel, [b] Contains 0.71 wt% P_2O_5

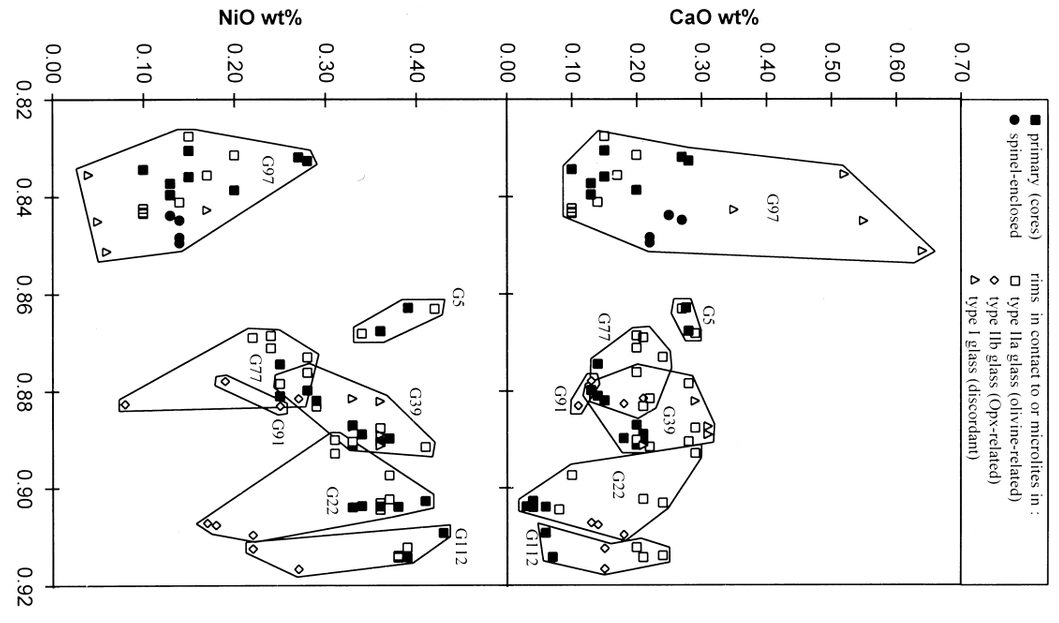

Fig. 2a, b Olivine compositions: Cores, rims against glasses and microlites within glass. Type I glass is brown and discordant; type II glass is clear (*IIa* between olivine crystals, *IIb* around orthopyroxene crystals). *Fields* encircle analyses from individual xenoliths. Note the Fe-enriched character of G97. Here, *white triangles* denote olivine microlites in interstitial glass in clinopyroxenite (partly phlogopite decompression glass). Note general enrichment of CaO in glass-equilibrated olivine (rims and microlites) in (**a**), and marked decrease in NiO in IIb glass microlites (**b**). This is consistent with a high degree of dissolution contamination to the IIb glass patches (see discussion)

other Eifel harzburgites (e.g. Dreiser Weiher: Stosch and Seck 1980). In the more strongly metasomatized harzburgite G77 both elements are decreased in Opx.

Clinopyroxenes

The clinopyroxenes display the most significant compositional variation with microtexture. An investigation of

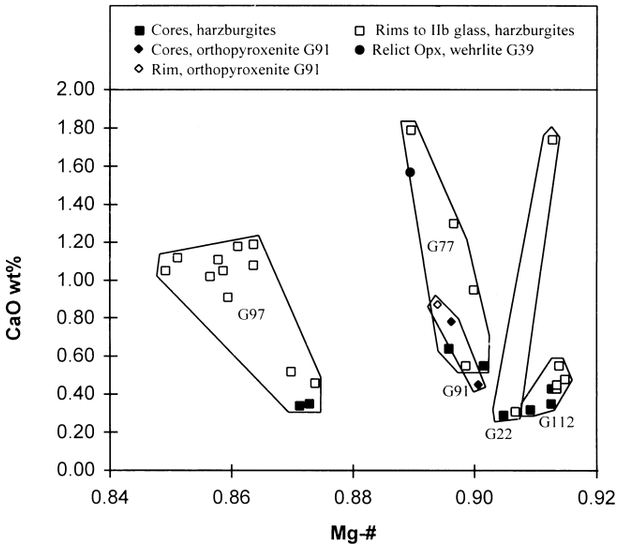

Fig. 3 Orthopyroxene compositions. *Fields* show analyses from individual xenoliths. Note CaO increase coupled with Mg-# increase in Opx rims in contact with type II glass in harzburgites. In sample G97, all analyses come from the lherzolite zone of wallrock, being divided from a clinopyroxenite vein by an Opx-absent wehrlite zone. Here, the low-CaO analyses are cores + rims of large opx prophyroblasts, the high-CaO group represents small opx neoblasts at the border to the wehrlite zone

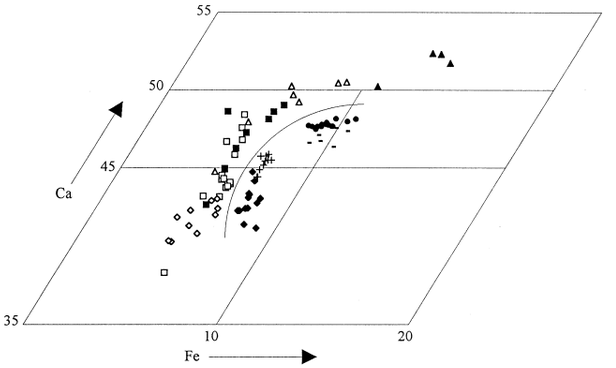

Fig. 4 Clinopyroxene compositions (Symbols as in Fig. 2, 3) plotted on an enlarged section of the Ca-Fe-Mg triangle. Note little scatter of Cpx Mg-# in various harzburgite and wehrlite xenoliths *(squares)* in contrast to ol + opx (Fig. 2, 3). Also, note Ca-depletion in IIb-glass-associated Cpx microlites, and Ca-enrichment in type I glass microlites. All analyses to the *right* of *curved line* are from composite xenolith G97, which consists of a phlogopite clinopyroxenite vein (*dots*) sundered from its lherzolite wall rock (*diamonds*) by a succession of massive phlogopite (*dashes*) and fine-grained wehrlite (*crosses*) zones

Cpx in Eifel lavas (Duda and Schmincke 1985) established a complex variability of compositions related to different depths and environments of crystallization (primary xenolith and metasomatic clinopyroxene, high-pressure and low-pressure cumulates). This makes the clinopyroxene chemistry in the Gees xenoliths particularly informative in assessing the genesis of the associated metasomatic textures and glasses.

Cpx compositions analysed in this study are plotted in the pyroxene quadrilateral in Fig. 4. There are significant variations between the different textural groups. Within the most primitive harzburgite sample studied here (G112), Cpx occurs only as microlites within the type II (clear) glasses. It shares a common chemical signature with similar microlites in all xenoliths where this glass type occurs, being enriched in Cr, Al but not in Ti. Its Mg-# is similar or slightly higher than those of associated olivine microlites. As is the case with the olivine microlites, the Mg-# of Cpx microlites in type IIb glass are the highest found (0.90–0.93). A significant difference between Cpx microlites in IIa and IIb glass patches is the decreased CaO content in the latter (Fig. 4, see Tables 2–4), whereas the CaO content of the inter-olivine (IIa) microlites is virtually indistinguishable from that of coarse Cpx crystals in the Gees suite. Coarse clinopyroxenes within the less refractory harzburgites (G77) and the Cpx dunite/wehrlite are less magnesian (0.85–0.90) than the microlites. Compared to the grouping of clinopyroxene types of Duda and Schmincke (1985), both coarse metasomatic Cpx and Cpx microlites in glass correspond to the Cr-diopside group inferred to be of sub-Moho origin.

In strong compositional contrast to this group are the clinopyroxenes from the cumulate clinopyroxenites, the clinopyroxene microlites within type I (brown) glass and the clinopyroxene reaction rims around the xenoliths. All of these are markedly lower in Mg-#, enriched in CaO and share a high-Ti, Al and low-Cr signature. In detail, however, the clinopyroxenes associated with type I glass can be distinguished from the cumulate clinopyroxenes by differing Ti/Al ratios and particularly by a Na depletion trend compared to elevated Na levels within the cumulate clinopyroxenes. Coarse clinopyroxenes within the xenoliths display complex, sometimes oscillatory growth zoning patterns when in contact with type I glass veins (see Tables 2, 5). Both clinopyroxene microlites in the type I glass and in the clinopyroxene reaction rims around the xenoliths correspond chemically to the titanaugite group of Duda and Schmincke 1985, which they held to represent crystallization from the host magma during ascent through the crust.

Glass compositions

In broad terms, the compositions of glasses analysed in this study are consistent with the results of Edgar et al. (1989). However, a much more precise evaluation of the large compositional variability of the glasses is possible taking into account the detailed petrographic observations given above. Fig. 5 gives major element oxide variation trends plotted against MgO for the petrographically defined different glass types. From this figure it is clear that the marked oxide-oxide correlations found by Edgar et al. (1989) can be resolved into two compositional

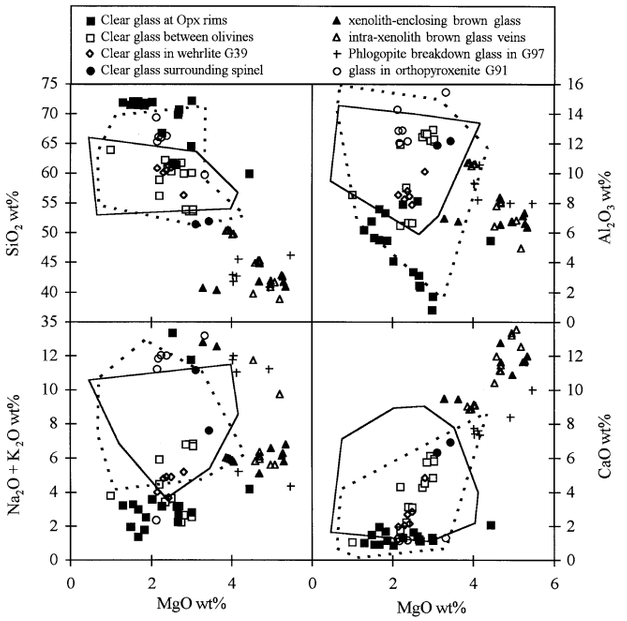

Fig. 5 Major-oxide variation diagrams for the various textural varieties of Gees glasses. *Squares* are glass analyses from harzburgites. Shown for comparison, field of Si-Al-rich glasses of Schiano and Clocchiatti (1994) *(solid line)* and Si-Al-rich glasses in xenoliths possibly related to carbonatite metasomatism (*dotted line*, data of Dautria et al. 1992; Ionov et al. 1993; Hauri et al. 1994)

apices. The type IIb glass patches associated with orthopyroxene decomposition represent an extremely Si and Al rich end member. In contrast the type I glasses, which discordantly infiltrate the xenoliths, are strongly silica undersaturated and mafic. It must be stressed, however, that the overall variation trend in the oxide-oxide plots is not a mixing trend. Mixing as observed optically by colour change is restricted to few tens of microns at many contacts between type I and type II glasses. In the harzburgites, the difference between type IIa and type IIb glasses is significant. The former, which are in contact only with olivine, are markedly less silica-rich, but frequently richer in alkalies than the IIb glasses in contact with orthopyroxene. Moreover, inter-olivine glass compositions are variable from xenolith, whereas IIb glasses in all xenoliths have a comparatively constant composition.

The Na, K and Cl variations within individual xenoliths are important since they are the components with the highest diffusivity in the melt. Invariably, Na and K are higher in the discordant type I glass than in the peraluminous clear glasses (type II). According to experimental studies in which mafic and felsic melts were equilibrated (Watson 1976), the opposite would be expected if there had been significant equilibration between type I and type II glasses in the Gees xenoliths after infiltration of the type I glass veins. Similarly, the Cl concentration in the type II, intraxenolithic glass compared to those in the extraxenolithic type I glass vary in a manner which is hardly consistent with either diffusive re-equilibration of the glass types or bulk Cl loss by degassing after eruption of the xenoliths. Thus, chemical evidence supports the interpretation already derived from petrographic characteristics that the type II glass represents an independent melt variety whose origin and composition is related exlusively to intraxenolith assemblages.

Assessment of disequilibrium between glasses and xenolith phases

If the intraxenolithic type II glasses formed by some equilibrium process within the xenoliths, their Mg-# must correspond to the known K_D(Fe/Mg) for olivine-melt. As the Mg-# of the olivines ranges from 0.92 in the most refractory xenoliths to 0.86 in metasomatized harzburgites and wehrlites, equilibrium melts would have Mg-# of 0.78 to 0.65 using a K_D value of 0.3. The type I glasses enclosing and infiltrating the xenoliths have far lower Mg-#, typically between 0.4 and 0.5 (neglecting Fe^{3+}, see below). In contrast, the Mg-# of the type II glasses is invariably higher (see Tables 2 to 7). It is highest in the most Si-Al-enriched subgroup (IIb) associated with orthopyroxene (typically between 0.55 and 0.65). Thus, type II glasses are distinctly closer to equilibrium with their host xenoliths than the infiltrating type I glass. This is even more evident if one takes ferric iron into consideration. Kilinc et al. (1983) have given a semi-empirical equation allowing estimation of Fe^{3+} contents of basaltic glasses. According to their calibration and using a temperature of 1150° C and an oxygen fugacity of the NNO buffer, $Fe^{3+}/\Sigma Fe$ ratios in the xenolith-enclosing type I glass cluster around 0.20 compared to 0.10 in most type II glasses. A more oxidised state of the type I glasses is in agreement with the fact that their quench spinel is significantly richer in ferric iron than that of the type II glasses: see Table 2 versus Table 5. The corrected Mg-# of the type I glasses then is 0.52 and thus still far out of equilibrium with the xenoliths, whereas those of the IIb glasses attain values of 0.60 to 0.67. Although these values do not represent equilibrium, they are not far removed from it – in concordance with the petrographical observation that olivine has smooth surfaces in contact with type II glasses, but ragged, etch-pit rich surfaces in contact with the infiltrating type I glass veins.

Discussion

Origin of the type II glasses

An assessment of the metasomatic agent responsible for the harzburgite-to-wehrlite transformation in the Gees suite hinges on the significance of the intergranular, silica-rich type II glasses. As discussed above, there has been minimal interdiffusion between both melt types. Thus, compositions of the latter cannot be explained by

Table 8 Reconstruction of mantle precursor to type II glass in harzburgite G112. Method of calculation: Bulk compositions have been calculated from the modal analyses in Table 1, using the mineral compositions of Table 2 (normalized to 100 except glass). Melts have been calculated by subtracting primary phases (Table 1) in the denoted mass proportions until the Mg-# of the residual reached 0.75, and renormalized to 100. For Spinel, in the absence of own data, analysis 3, table 8 of Lloyd et al. (1991) has been used; their xenolith FL86 is similar to G112 of this study. Melt 3 has been calculated by varying the olivine/spinel ratio in the subtracted component until renormalized Cr_2O_3 in the melt reached 0.60 wt%. Kelemen model melts are taken from Table 3 in Kelemen (1990) and Table 8b in Kelemen et al. (1990)

	a) Type IIa melt patches including spl microlites				b) Type IIa melt patches neglecting spl microlites			c) Type IIb melt patches		d) Kelemen (1990) model melts	
	Bulk	Calculated melts			Bulk	Calculated melts		Bulk	Melt	Calculated MHAB 1238	Experimental 1150-1
		1	2	3		4	5		6		
SiO_2	51.90	54.71	55.17	58.01	55.97	60.26	60.84	57.91	59.50	58.09	50.70
TiO_2	0.12	0.15	0.15	0.14	0.12	0.16	0.16	0.05	0.10	0.82	3.30
Al_2O_3	14.81	18.57	18.60	17.63	13.76	17.67	17.70	7.18	15.15	17.04	18.40
Cr_2O_3	3.11	3.89	3.56	0.60	0.39	0.50	0.09	0.48	0.74		0.00
Fe_2O_3	0.63	0.79	0.73	0.22	0.17	0.22	0.15	0.06	0.14	0.25	1.30
FeO	4.35	3.27	3.19	2.84	3.87	2.52	2.42	4.06	1.22	1.34	5.00
MnO	0.07	0.05	0.05	0.05	0.06	0.04	0.04	0.07	−0.04		0.10
NiO	0.07	−0.01	−0.01	0.01	0.06	−0.03	−0.03	0.08	0.11		0.00
MgO	14.50	5.51	5.36	7.14	14.35	4.25	4.07	21.39	2.05	6.65	4.70
CaO	8.77	10.98	11.09	11.23	9.45	12.11	12.24	7.75	18.61	12.58	9.80
Na_2O	0.82	1.02	1.03	1.05	0.88	1.13	1.14	0.49	1.20	2.62	3.00
K_2O	0.67	0.84	0.85	0.86	0.72	0.93	0.94	0.41	1.02	0.64	0.70
Cl	0.18	0.22	0.22	0.23	0.19	0.24	0.25	0.08	0.21		
Σ	100.00	100.00	100.00	100.00	100.00	100.00	100.00	100.00	100.00	100.03	97.00
Mg#	0.856	0.750	0.750	0.818	0.869	0.750	0.750	0.904	0.750	0.898	0.626
Melt Fraction	0.80	0.79	0.78		0.78	0.77		0.40			
Subtracted phases:											
Opx		0	0	0		0	0		100		
Ol		100	97	74		100	97		0		
Spinel		0	3	26		0	3		0		

interaction with extraxenolithic melts. Furthermore, their incompatible element budget (Fig. 5) cannot be derived from any melting (decompressional or otherwise) of simple four-phase spinel lherzolite. Amphibole breakdown has been ruled out above on the basis of the absence of amphibole to the Gees suite. Additionally, the bulk composition of both the IIa and IIb melt glass + microlite patches (Table 8) does not conform well to amphibole compositions, and as they occur together with phlogopite that is little affected by melting, it would be difficult to envisage why amphibole broke down completely, but not phlogopite. Glass in existing melt pools around phlogopite (Table 7) typically is low in silica, being in many respects more similar to the type I glass. This strongly disfavours an origin of the intraxenolithic glasses by decompressional melting of phlogopite. As this is consistent with the observation that some phlogopite rich xenoliths (G5) are essentially glass-free, whereas phlogopite-free harzburgites may have large amounts of intergranular glass even though both share a similar *P–T* decompression history, we reject melting of a hydrous phase as the principal source of the glass. Thus, the type II glass must have originated from a precursor melt present within the xenoliths at mantle depths. However, the composition of the type II glasses is grossly inconsistent with available experimental data on equilibrium melting in the mantle (e.g. Fuji and Scarfe 1985; Falloon et al. 1988; Hirose and Kushiro 1993), being essentially high-alumina andesitic with normative quartz + corundum + hypersthene and following an calc-alkaline trend. Either the glasses must have been greatly modified during ascent of the xenoliths or some other process than equilibrium melting must be responsible for their formation.

Mass-balance calculations

We have tried to estimate the contribution of post-entrainment melt modification during ascent in the case of the harzburgite G112, which is free of phlogopite and metasomatic Cpx so that possible decompressional contaminants can only be olivine, Opx and spinel. If a melt was present at mantle depths in this sample, it may have been modified during ascent by two processes: dissolution of surrounding phases (Ol, Opx) and crystallization of the microlites now observed. Both would change the bulk composition of the melt patches. From modal analyses of the melt patches (Table 1), we calculated bulk compositions for the type II melt patches both around Opx (IIb) and between olivines (IIa) (see Table 8). Both have Mg-# far too high to be in equilibrium with primary phases, indicating that their bulk composition in-

cludes a significant component of dissolution of neighbouring phases during ascent. As the Mg-# of the olivine in harzburgite G112 is 0.912, the melt patches must have had a Mg-# of 0.73–0.77 prior to dissolution modification, assuming Fe-Mg exchange equilibrium. From this, the composition of the melt prior to dissolution of its neighbouring phases can be calculated. To obtain limiting values, we assumed that this unmodified melt had a Mg-# of 0.75, and that it dissolved only Opx in the case of the IIb patches and only olivine in the case of the IIa patches. From this, we calculated the composition of pre-dissolution melts by subtracting Opx respective to olivine until the Mg-# of the residual reached a value of 0.75. However, the IIa patches contain a small but significant amount of Cr-rich spinel microlites, so that errors in our modal estimate introduce large errors in the bulk Cr_2O_3 content of the patches and of the calculated initial melts (see Table 8, melt 1). The presence of these Cr-rich spinel microlites, and the Cr-rich compositions of the Cpx microlites, also may indicate that the melt patches were also modified by dissolution of primary spinel. Therefore, we tested the robustness of this mass-balance calculation by (1) neglecting spinel microlites in the calculation of IIa bulk compositions; (2) including 3% primary spinel in the subtracted (assimilated) component; (3) calculating a melt from the IIa bulk composition by arbitrarily assuming an initial content of 0.6 wt% Cr_2O_3 in the melt (Table 8 melt 3). The results of these calculations are summarized in Table 8, which also gives the mass fraction of calculated initial (pre-modification) melt in the bulk composition of IIa and IIb glass + microlite patches.

The compositions of the melts thus calculated (Table 8) are remarkably coherent for the different assumptions. All melts are characterized by high contents of SiO_2 (55–60 wt%) and Al_2O_3 ($\approx$18 wt% for the IIa patches). Notably, the Al content does not depend significantly on the treatment of spinel in the calculation assumptions, nor does the melt fraction. The result of the calculation for the IIb patches associated with Opx breakdown is probably least correct, as the exclusion of olivine as a contaminating phase is certainly incorrect, and it yields an unrealistically high content of CaO. This is a consequence of the bulk Mg-# of this type of patch being nearly as high as that of primary xenolith Opx. Here, it should be noted that the adopted approch of mass-balance calculation implies that all of the microlites formed during decompression and were not present at mantle depth. However the type II melt is associated with the transformation of harzburgites into wehrlites, and a part of the microlites may have crystallized already in the mantle from a melt consuming Opx in an AFC-type reaction. Inclusion of these into the bulk composition of melt patches in our calculation enhances their Mg-# and produces too high degrees of contamination. This effect would be expected to be most prominent in the IIb glass patches. Also, this would imply that true melt compositions lie between those calculated here and those measured by microprobe, i.e. are even more Si-Al-rich than the results of our calculations. In spite of these uncertainties, we note that the low melt fraction calculated for the IIb patches is in accordance with the petrographical observation that glass-Opx boundaries are far more irregular than Ol-glass. We conclude that the type II glasses in the harzburgite xenolith G112 (taken as an example for the Gees suite) did not originate from decompressional melting, but were only modified by it, and that their mantle precursor had a markedly calc-alkaline character.

We suggest that this mantle precursor to the type II glasses in the Gees xenoliths originated within the mantle by silicate melt-harzburgite reactions similar to those envisaged in the model of Kelemen (1990), which explains the genesis of calc-alkaline melts in the shallow upper mantle by AFC-type reactions between tholeiite and wallrock. Our estimates of the precursor to the type II Gees glasses are strikingly similar to the compositions of high-Al andesites produced in Kelemen's model (see Table 8). Thus, the Gees suite may provide evidence for the actual applicability of this model. It must be stressed that according to this interpretation, the reconstructed melt, which is associated with the metasomatism in the Gees suite (transformation from harzburgite to wehrlite), is itself the hybridization product and is not the melt which initially started to react with the mantle wallrock. This primary melt reacting with the sub-Eifel harzburgites is unlikely to have been tholeiitic, as erupting lavas are alkaline basalts, foidites and basanites (Mertes and Schmincke 1985). Melt inclusion trails in Opx in the least metasomatized Gees harzburgites exclusively have type I (brown) glass which is a strongly silica-undersaturated basanitic melt, though not a primitive one according to its low Mg-# ($<$0.5).

Derivation of silica activity from olivine + clinopyroxene microlites

The reactivity of a metasomatizing melt with respect to orthopyroxene depends critically on its silica activity. Low-$a\mathrm{SiO_2}$ melts are increasingly further from equilibrium with Opx when rising to shallow mantle levels and there must be especially prone to wallrock reaction. To obtain information about the $a\mathrm{SiO_2}$ of the melt reacting with the Gees harzburgite to produce the andesitic hybrid melt now represented by the type II glass, we used olivine-pyroxene compositions in the Gees xenoliths. Exchange equilibria between olivine and pyroxenes can serve as buffers for silica activity:

$$(Mg_2SiO_4)_{OL} + SiO_2 = (Mg_2Si_2O_6)_{CPX} \quad (1)$$

$$(CaMgSiO_4)_{OL} + SiO_2 = (CaMgSi_2O_6)_{CPX} \quad (2)$$

However, reaction (1) has a degree of freedom less than (2) as in the latter Ca is an additional component. Thus, (1) fixes $a\mathrm{SiO_2}$ at given *P, T,* whereas $a\mathrm{SiO_2}$ in (2) is dependent on bulk composition (X_{CA}) of the phases. We modelled these silica buffers using the program QUIlF of Andersen et al. (1993). The results are shown in Figs. 6

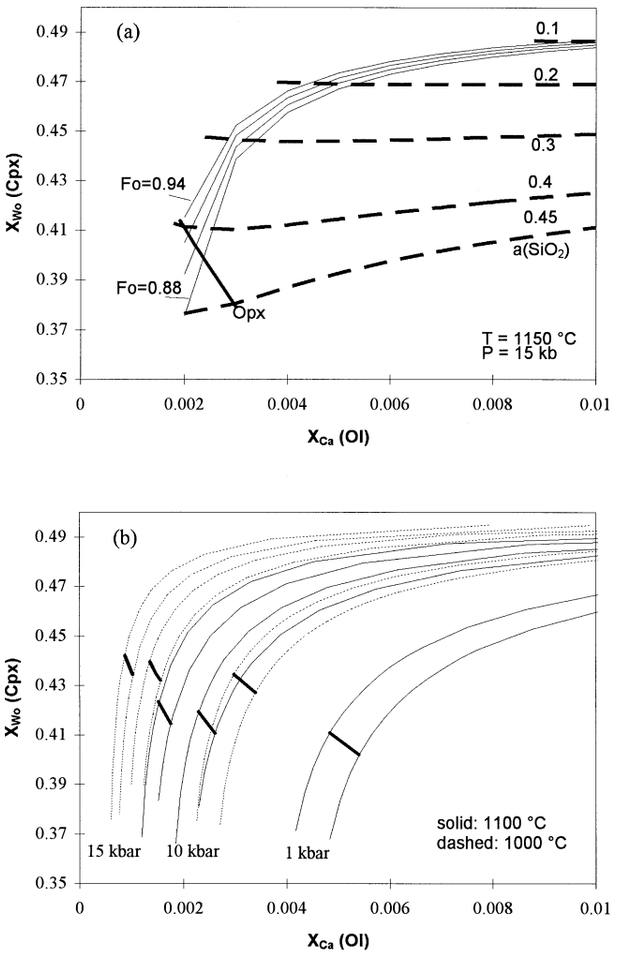

Fig. 6 Equilibrium Ca concentrations in coexisting Ol + Cpx as function of X_{fe}, *P, T* and $aSiO_2$. *Thin solid lines* in *upper* diagram (**a**) connect equilibrium compositions as a function of silica activity at Mg-# of 0.88 to 0.94 in olivine, calculated using the program QUI1F of Andersen et al. (1993). *Thick dashed lines* indicate silica activity isopleths, along which *X*Fe varies. *Thick solid line "Opx"* gives the position of the Ol-Cpx-Opx buffer at the specified conditions. Above this line, Opx is unstable, below it, Ol is unstable. The *lower* diagram (**b**) summarizes the effects of *P, T* on the Ol + Cpx compositions. Bands of equilibrium compositions similar to that in the upper diagram are outlined, at different *P, T* as indicated, the *left* margin of which corresponds to Fo_{94} olivine, and the right to Fo_{88}. *Thick line* on each band depicts the position of the Ol + Opx + Cpx silica buffer. Note that isothermal decompression tends to decrease the Ca content of Cpx, while isothermal, isobaric metasomatism by an opx-undersaturated agent (carbonatite or silicate melt) strongly increases Ca in Cpx

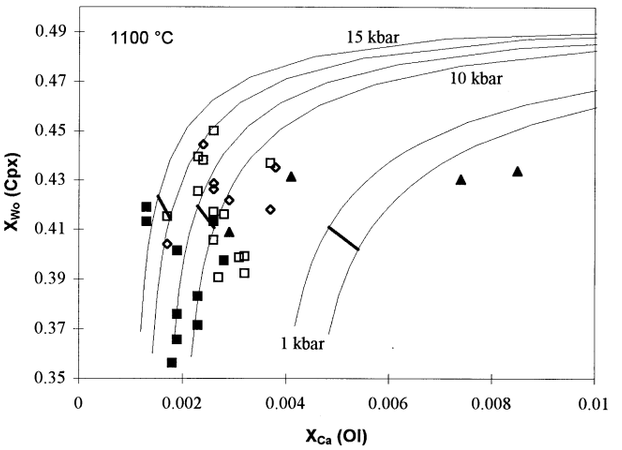

Fig. 7 Compositions of Ol + Cpx microlite pairs in the Gees glasses superimposed on a silica activity dependent grid similar to Fig. 6. Symbols correspond to the enclosing glass types, see Fig. 5. *Thick line* on each of the three bands for 1, 10 and 15 kbar gives the opx-buffered compositions. Note that microlites from type IIb patches (Opx-associated) fall *below* the buffer lines, indicating equilibration at still higher temperature than that used for calculation of the bands, and that type IIa microlites from the same samples plot at a position consistent with low silica activities (Opx-undersaturation)

and 7. In Fig. 6a, reaction (2) defines lines of equilibrium Ca contents in coexisting olivine + Cpx at given *P, T,* and Mg-# of phases (see also Fig. 12 in Davidson and Lindsley 1989). The Ca content is expressed as X_{WO} in Cpx (calculated according to Lindsley and Anderson 1983), and X_{CA}=Ca/(Ca+Mg+Fe) in olivine. Variation in the Mg-# of phases (Fo_{88}–Fo_{94}) produces a band of equilibrium X_{WO}/X_{CA} values in Fig. 7 for each set of *P* and *T*.

Along such a band, the silica activity, contoured by dashed lines, decreases with increasing Ca concentration in both Ol and Cpx. If Opx coexists with Ol+Cpx, it fixes the silica activity, varying only slightly with Mg-# of phases. The Ca concentrations in equilibrium with this "lherzolite $aSiO_2$ buffer" vary with *P* and *T*. This variation is given in Fig. 6b as a set of heavy lines.

As Ol+Cpx crystallized as microlites from all type II glass patches in the Gees xenoliths, their compositions can be used in this way to record silica activities. The IIb patches are associated with Opx breakdown in the harzburgites, so silica activity is constrained to be Opx buffered. However, the microlite compositions of IIa glass patches differ markedly from those of IIb glass patches (see Table 2; CaO in Cpx microlites) within single harzburgite xenoliths, indicating that equilibrium during metasomatism was not maintained over distances of several millimeters. Thus, silica activity in purely olivine enclosed melt patches (type IIa) in the harzburgites is *not* constrained by Opx. The different Ol+Cpx microlite compositions in the various glass types of Gees are plotted in a X_{WO}–X_{CA} diagram (Fig. 7), and compared to equilibrium bands for 1, 10 and 15 kbar at a temperature of 1100° C, calculated in the same way as Fig. 6.

Two significant features must be stressed relating to this plot. Firstly, the Ol+Cpx microlite pairs from IIb glass patches, associated with Opx, have systematically lower Ca concentrations than others, plotting at or below the Opx buffer on Fig. 7 and at higher relative silica activities than others. The X_{WO} position of the Opx buffer is a strong function of temperature (compare Fig. 6). This reflects the strong increase of X_{EN} in Cpx with increasing

T in two-pyroxene assemblages, which is the basis of two-pyroxene thermometry. Thus, the deviation of many IIb microlite pairs below the Opx buffer in Fig. 7 may indicate a higher equilibration temperature, which would also shift the *P* bands in Fig. 7 to higher X_{CA} in olivine. Secondly, the microlites in type II glass in the wehrlites and Cpx dunites all plot in the Opx-undersaturated field along the X_{WO}–X_{CA} bands. Significantly, the microlites in the type IIa glass patches within the harzburgites have similar Opx-undersaturated compositions to the wehrlite microlites. These facts are consistent with the interpretation that the harzburgite-to-wehrlite transition was effected by a melt with a silica activity considerably lower than the lherzolite buffer at ambient conditions, and that strong gradients in silica activity on the grain-size scale were present in the harzburgites prior to their entrainment. Thus, silica activity analysis argues against a tholeiitic melt as that which via AFC reactions produced the calc-alkaline melt now reflected in the type II glass patches. In contrast, the strongly silica undersaturated nature of the xenolith-entraining lava of Gees neatly fits to the silica activities recorded by Ol+Cpx microlites in Fig. 7. Finally, it is to be noted that the type II glass microlites conform to high-pressure bands in the same xenoliths where some of the type I glass microlites plot at Ca concentrations only possible at low pressure of crystallization. This may indicate that many of the type II glass microlites indeed crystallized as AFC reaction products at depth, prior to decompression, as discussed above in conjunction with the mass-balance calculations.

Implications for other xenolith suites bearing Si-Al-rich glasses

As noted in the introduction, carbonatite melts have gained increasing attention as possible metasomatic agents in upper mantle peridotites. One of the reasons for this is that carbonatite melt may react with Opx in lherzolites to form Cpx+carbon dioxide, as has been found in experimental studies (e.g. Wallace and Green 1988) of CO_2-bearing peridotite assemblages. Thus metasomatism producing wehrlites may be conveniently explained invoking percolating carbonatite melt, especially if there is no strong Ti-Fe enrichment which is generally assigned to interaction with basaltic melt, and if the metasomatic products have high levels of Ca (e.g. Olmani: Rudnick et al. 1993; Gees: Dalton and Wood 1993). This led Thibault et al. (1992) to suggest that the Gees suite could be related to carbonatite metasomatism. However, from the petrographical observations of this study and the discussion of the significance of the type II glasses in the Gees suite, it is apparent that the metasomatism in Gees can fully be explained by reactions between Opx-undersaturated silicate melt and harzburgite, during which a distinct Si-Al-rich hybrid melt was produced. As evidence for involvement of carbonatite melts is lacking, we reject them as possible agents in the case of the Gees suite. According to olivine-pyroxene equilibria (Figs. 6, 7), high-Ca compositions of Cpx and olivine are simply a consequence of low silica activity in the metasomatic agent. Thus they cannot be used as independent evidence to differentiate between metasomatism by carbonatite melt and by opx-undersaturated silicate melt.

Silicate glasses, Si-Al rich that are compositionally quite similar to the type II glass of Gees have been frequently reported in xenolith suites. They have also been found in many of the xenolith suites in which metasomatism has been explained by carbonatitic melts (Yaxley et al. 1991; Dautria et al. 1992; Rudnick et al. 1993; Ionov et al. 1993; Hauri et al. 1994). A recent survey has demonstrated that similar Si-Al-rich glasses have a world-wide distribution, occurring in xenoliths of oceanic islands as well as intraplate alkaline provinces, and that at least some of these melts have been metasomatically active (Schiano and Clocchiatti 1994). In most cases, however, this type of glasses has not been considered as being a remnant of possible metasomatic agents, but rather has been discarded as a decompressional disequilibrium melting product, due to its Si-Al-rich character, which is an improbable composition for mantle melts taken at face value. A compilation of these glass data is

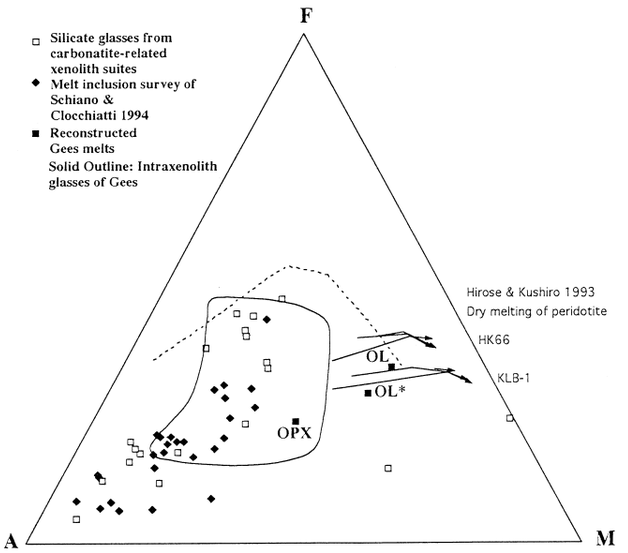

Fig. 8 Comparison of Gees glasses with Si-Al-rich (broadly "andesitic") glasses from the compilation of Schiano and Clocchiatti (1994) and from xenoliths suggested to be related to carbonatite metasomatism (Jones et al. 1982; Dautria et al. 1992; Ionov et al. 1993; Hauri et al. 1994). *Outlined field* includes all type I and II glasses from this study. *Black squares* are the reconstructed compositions of mantle melt from which type II glass in harzburgite G112 is possibly derived (taken from Table 8). These are: *OL:* based on IIa glass patches including spinel microlites; *OL*:* based on IIa glass patches neglecting spinel microlites; *OPX:* based on type IIb glass patches associated with Opx. *Lines* with *arrows* give the compositions of experimentally produced dry partial melts of peridotite (Hirose and Kushiro 1993), using two different bulk compositions. Each *line* gives the evolution of partial melt with increasing melt fraction (≈temperature) at a specific pressure (10, 15, 20 kbar). Note that OL and OL* plot near possible partial melt compositions, but still are calc-alkaline

given on an AFM plot in Fig. 8, together with the field of type II glass compositions from Gees and its inferred precursor melt in Gees xenolith G112 (from Table 8). All of the glasses fall in the calc-alkaline field, and most are far removed from (dry) equilibrium melts (e.g. Hirose and Kushiro 1993, also given in Fig. 8). For the Gees suite, we have shown that the compositions of these glasses as observed today do indeed reflect dilution by a decompressional component, but that pre-eruptive melt compositions can be reconstructed which can be explained by AFC-type reactions as envisaged by Kelemen (1990) and Kelemen et al (1990). By analogy, similar silicate melt-peridotite interactions may play a significant role in many other suites, including those where carbonatite metasomatism has been inferred using geochemical data (selective LREE enrichment, trace element ratios like Zr/Hf). If the presence of glasses comparable to the type II glasses of Gees in some of these suites (e.g. Dautria et al. 1992; Hauri et al. 1994) is due to similar interactions with undersaturated (alkaline) silicate melts, it is conceivable that this would also significantly have affected their trace element contents. In these cases a reinvestigation of the glass-forming processes seems warranted to separate their geochemical effects from those of possible carbonatite metasomatism. As a starting point, an investigation of the trace element characteristics of the Gees glasses is currently under way.

Conclusions

1. Detailed petrography of glass-crystal relationships in the Gees xenoliths reveals that the glasses described by Edgar et al. (1989) can be divided in two groups of different origin: type I glass infiltrating into the xenoliths and type II glass exclusively derived from the xenolith's interior.

2. Type I glass is strongly silica undersaturated and similar to the host magma entraining the xenoliths. Type II glass is variably enriched in A1 and Si and has broadly andesitic compositions. This glass can further be subdivided into extremely Si enriched glass related to Opx breakdown in harzburgites (type IIb, up to 72 wt% SiO_2), and less silicic intergranular glass between olivine $\pm$ clinopyroxene (type IIa) in all samples.

3. Type II glass is derived from a melt of mantle origin. Its composition cannot be explained by melting of xenolith phases nor by infiltration from xenolith-entraining magma. It has been extensively modified during ascent by dissolution of Ol$\pm$Opx and by crystallization of microlites (mainly Ol+Cpx). These processes are responsible for the observed silica enrichment. However, the pre-eruption melt can be estimated to be a high-alumina basaltic andesite (55–60 wt% SiO_2, 18 wt% Al_2O_3, 2 wt% alkalies).

4. The mantle melt from which the type II glass is derived was highly reactive with respect to Opx. Chemical and petrographical data show that the harzburgite-to-wehrlite metasomatism in Gees can be explained fully by AFC-type reactions between strongly opx-undersaturated silicate melt and harzburgite wall rock similar to those proposed by Kelemen (1990). No evidence for a participation of carbonatite melts has been found, so that a connection of the Gees suite to carbonatite metasomatism as proposed by Thibault et al. (1992) is not supported.

5. High-Ca compositions of Ol+Cpx simply reflect low activities of silica and cannot be taken as unequivocal evidence for metasomatism by carbonatite. In contrast, type II Gees glasses are similar to unusual calc-alkaline glasses present in many xenolith suites which have been explained as resulting from carbonatite metasomatism. In these suites, reactions between low-$a$$SiO_2$ silicate melts (instead of carbonatites) and harzburgite could play a major role.

Acknowledgements Funding for this work by the Deutsche Forschungsgemeinschaft is gratefully acknowledged (grants Fo 181/3-1, Fo 181/3-2, Gerhard Hess Programm). Manfred van Bergen is thanked for providing access to the microprobe facilities at the Institut voor Aardwetenschappen, Rijksuniversiteit Utrecht, and Tilly Bouten for assistance with the microprobe. Stimulating discussions with Sieger van der Laan greatly helped in developing the concepts set out here. Also, we greatly benefitted from the use of the QUI1F program of Andersen et al. (1993) summarizing the olivine-pyroxene modelling by the Lindsley group in a very convenient form.

References

Andersen DJ, Lindsley DH, Davidson PM (1993) QUI1F: A PASCAL program to assess equilibria among Fe-Mg-Ti oxides, pyroxenes, olivine and quartz. Comput Geosci 19: 1333-1350

Dalton JA, Wood BJ (1993) The compositions of primary carbonate melts and their evolution through wallrock reaction in the mantle. Earth Platnet Sci Lett 119: 511–525

Dautria JM, Dupuy C, Takherist D, Dostal J (1992) Carbonate metasomatism in the lithospheric mantle: peridotitic xenoliths from a melilitic district of the Sahara basin. Contrib Mineral Petrol 111: 37–52

Davidson PM, Lindsley DH (1989) Thermodynamic analysis of pyroxene-olivine-quartz equilibria in the system CaO-MgO-FeO-SiO_2. Am Mineral 74: 18–30

Duda A, Schmincke HU (1985) Polybaric differentiation of alkali basaltic magmas: evidence from green-core clinopyroxenes (Eifel, FRG). Contrib Minear Petrol 91: 340–353

Düren H (1984) Zur Petrologie der Mantelxenolithe von Gees (Westeifel) unter besonderer Berücksichtigung der Teilschmelzenbildung (unpublished). Diploma thesis, University of Köln

Edgar AD, Lloyd FE, Forsyth DM, Barnett RL (1989) Origin of glass in upper-mantle xenoliths from the Quaternary volcanics SE of Gees, West Eifel, Germany. Contrib Mineral Petrol 103: 277–86

Falloon TJ, Green DH, Hatton CJ, Harris K (1988) Anhydrous partial melting of a fertile and depleted peridotite from 2 to 30 kb, and application to basalt petrogenesis. J Petrol 29: 1257–1282

Frey F, Prinz U (1978) Ultramafic inclusions from San Carlos, Arizona: petrologic and geochemical data bearing on their petrogenesis. Earth Planet Sci Lett 38: 129–176

Fuji T, Scarfe CM (1985) Composition of liquid coexisting with spinel lherzolite at 10 kbar and the genesis of MORBs. Contrib Mineral Petrol 90: 18–28

Hauri EH, Shimizu N, Dieu JJ, Hart SR (1994) Evidence for hotspot-related carbonatite metasomatism in the oceanic upper mantle. Nature 365: 221–227

Ionov D, Dupuy C. O'Reilly S, Kopylova M, Genshaft Y (1993) Carbonated peridotite xenoliths from Spitsbergen: implications for trace element signature of mantle carbonatite metasomatism. Earth Planet Sci Lett 119: 283–297

Kelemen PB (1990) Reaction between ultramafic rock and fractionating basaltic magma. I. Phase relations, the origin of calc-alkaline magma series, and the formation of discordant dunite. J Petrol 31: 51–98

Kelemen PB, Joyce DR, Webster JD, Holloway JR (1990) Reaction between ultramafic rock and fractionating basaltic magma. II. Experimental investigation of reaction between olivine tholeiite and harzburgite at 1150–1050° C and 5 kbar. J Petrol 31: 99–134

Kilinc A, Carmichael ISE, Rivers ML, Sack RO (1983) The ferric-ferrous ratio of natural silicate liquids equilibrated in air. Contrib Mineral Petrol 83: 136–140

Hirose K, Kushiro I (1993) Partial melting of dry peridotites at high pressures: determination of melts segregated from peridotite using aggregates of diamond. Earth Planet Sci Lett 114: 477–490

Lindsley DH, Andersen DJ (1983) A two-pyroxene thermometer. Proc 13th Lunar Planet Sci Conf, J Geophys Res Suppl 88:A887–A906

Lloyd FE, Edgar AD, Forsyth DM, Barnett RL (1991) The paragenesis of upper-mantle xenoliths from the quaternary volcanics south-east of Gees, West Eifel, Germany. Mineral Mag 378: 95–112

Mertes H, Schmincke HU (1985) Mafic potassic lavas of the Quaternary West Eifel volcanic field. Contrib Mineral Petrol 89: 330–45

Rudnick RL, McDonough WF, Chappell BW (1993) Carbonatite metasomatism in the northern tanzanian mantle: petrographic and geochemical characteristics. Earth Planet Sci Lett 114: 463–475

Schiano P, Clocchiatti R (1994) Worldwide occurrence of silica-rich melts in sub-continental and sub-oceanic mantle minerals. Nature 368: 621–624

Stosch HG, Seck HA (1980) Geochemistry and mineralogy of two spinel peridotite suites from Dreiser Weiher, West Germany. Geochim Cosmochim Acta 44: 457–470

Thibault Y, Edgar AD, Lloyd FE (1992) Experimental investigation of melts from a carbonated phlogopite lherzolite: implications for metasomatism in the continental lithosphere. Am Mineral 77: 784–794

Wallace ME, Green DH (1988) Mantle metasomatism by ephemeral carbonatite melts. Nature 336: 459–462

Watson EB (1976) Two-liquid partition coefficients: experimental data and geochemical implications. Contrib Mineral Petrol 56: 119–134

Watson EB, Brenan, JM, Baker DR (1990) Distribution of fluids in the continental mantle. In: Menzies MA (ed) Continental lithosphere. Clarendon Press, Oxford, pp 111–125

Witt G (1989) Origin of amphibole in recrystallized mantle xenoliths from the Rhenish massif: implications for the nature of mantle metasomatism. Earth Planet Sci Lett 91: 327–340

Witt-Eickschen G, Seck HA, Reys C (1993) Multiple enrichment processes and their relationships in the subcrustal lithosphere beneath the Eifel (Germany). J Petrol 34: 1–22

Yaxley GM, Crawford AJ, Green DH (1991) Evidence for carbonatite metasomatism in spinel peridotite xenoliths from Western Victoria, Australia. Earth Planet Sci Lett 107: 305–317